

Magnetically tunable Dirac and Weyl fermions in the Zintl materials family

Anan Bari Sarkar,^{1,*} Sougata Mardanya^{1,2,*} Shin-Ming Huang,³ Barun Ghosh,⁴ Cheng-Yi Huang,⁴ Hsin Lin,⁵ Arun Bansil,⁴ Tay-Rong Chang,^{2,6,7} Amit Agarwal,^{1,†} and Bahadur Singh^{8,‡}

¹*Department of Physics, Indian Institute of Technology, Kanpur 208016, India*

²*Department of Physics, National Cheng Kung University, Tainan 701, Taiwan*

³*Department of Physics, National Sun Yat-sen University, Kaohsiung 80424, Taiwan*

⁴*Department of Physics, Northeastern University, Boston, Massachusetts 02115, USA*

⁵*Institute of Physics, Academia Sinica, Taipei 11529, Taiwan*

⁶*Center for Quantum Frontiers of Research and Technology, Tainan 701, Taiwan*

⁷*Physics Division, National Center for Theoretical Sciences, National Taiwan University, Taipei, 10617 Taiwan*

⁸*Department of Condensed Matter Physics and Materials Science, Tata Institute of Fundamental Research, Mumbai 400005, India*



(Received 9 September 2021; revised 4 April 2022; accepted 12 April 2022; published 28 April 2022)

Recent classification efforts encompassing crystalline symmetries have revealed rich possibilities for solid-state systems to support a tapestry of exotic topological states. However, finding materials that realize such states remains a daunting challenge. Here, we show how the interplay of topology, symmetry, and magnetism combined with doping and external electric and magnetic field controls can be used to drive the SrIn₂As₂ materials family into a variety of topological phases. Our first-principles calculations and symmetry analysis reveal that SrIn₂As₂ is a dual topological insulator with $Z_2 = (1; 000)$ and mirror Chern number $C_M = -1$. Its isostructural and isovalent antiferromagnetic cousin EuIn₂As₂ is found to be an axion insulator with $Z_4 = 2$. The broken time-reversal symmetry via Eu doping in Sr_{1-x}Eu_xIn₂As₂ results in a higher-order or topological crystalline insulator state depending on the orientation of the magnetic easy axis. We also find that antiferromagnetic EuIn₂P₂ is a trivial insulator with $Z_4 = 0$, and that it undergoes a magnetic-field-driven transition to an ideal Weyl fermion or nodal fermion state with $Z_4 = 1$ with applied magnetic field. Our study identifies Sr_{1-x}Eu_xIn₂(As, P)₂ as a tunable materials platform for investigating the physics and applications of Weyl and nodal fermions in the scaffolding of crystalline and axion insulator states.

DOI: [10.1103/PhysRevMaterials.6.044204](https://doi.org/10.1103/PhysRevMaterials.6.044204)

I. INTRODUCTION

Since the discovery of Z_2 topological insulators, exploring the role of crystalline symmetries in protecting the nontrivial topology of Bloch Hamiltonians more generally has become a topic of intense research [1–4]. The interplay of symmetry and topology in the crystalline solids gives birth to many new topological insulators and metals, such as the mirror (glide-mirror)-protected topological crystalline insulators (TCIs) [5,6], rotational-symmetry-protected TCIs [7,8], higher-order topological insulators [9,10], Dirac [11–13], Weyl [14–16], and unconventional fermion semimetals [17–20], among other possibilities [21,22]. The TCIs are characterized by a unique set of topological invariants which depend only on the dimension and symmetry of the crystalline group [21,22]. The associated topological properties remain robust under symmetry-protecting perturbations and provide materials platforms for developing next-generation low-power-consuming high-speed electronic, optoelectronic, and spintronic devices [23,24]. The need for finding new classes of tunable

topological materials in order to fill the critical gap in the available materials families is thus clear.

The manipulation of quantum interactions and topology in the crystalline matrix can provide a promising route for tuning the topological properties of materials. The recent discovery of topological magnets in which the nontrivial topology is intertwined with magnetism suggests that certain topological responses could be tuned through external electric and magnetic fields [25–30]. The topological state in the currently available topological magnets, however, originates from the underlying paramagnetic state and for this reason these materials allow only limited tunability. It is highly desirable, therefore, to find new strategies for identifying tunable topological materials.

A natural paradigm for discovering new tunable topological materials is to exploit the strong interplay between magnetism and topology in families of isovalent and isostructural materials. Such materials families can offer great flexibility with respect to magnetism, topology, chemical composition, lattice parameters, and transport properties. In particular, spatial and nonspatial symmetries of the parent materials can be relaxed by introducing magnetism with ionic substitutions or crystal structure engineering in a topological nonmagnet to drive various different types of topological magnetic orders [31,32]. Using this approach as a

*These authors contributed equally to this work.

†amitag@iitk.ac.in

‡bahadur.singh@tifr.res.in

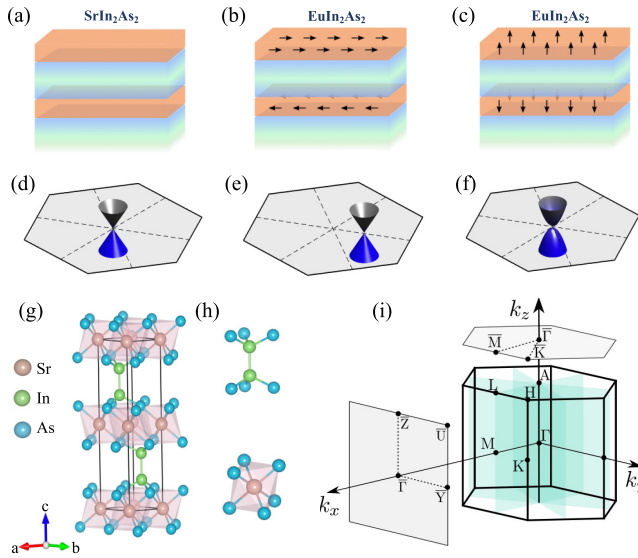


FIG. 1. Methodology to design magnetically tunable topological states and crystal structure. (a)–(f) Schematics of the evolution of the topological surface states as we break the mirror and time-reversal symmetries. (a), (d) In the presence of both time-reversal and mirror symmetry in the nonmagnetic SrIn_2As_2 , the gapless Dirac point appears at the $\bar{\Gamma}$ point. (b), (e) With time-reversal symmetry broken but mirror symmetry intact in aAFM EuIn_2As_2 , the gapless Dirac point is pinned to the mirror-symmetric line but shifts away from the $\bar{\Gamma}$ point. (c), (f) On breaking the time-reversal symmetry and the mirror symmetry in cAFM EuIn_2As_2 , the surface states become gapped at the $\bar{\Gamma}$ point. (g), (h) Crystal structure of Zintl $\text{Eu}/\text{SrIn}_2\text{As}_2$ family showing stacking of the layers of individual atoms along the c axis. (i) Bulk and projected (001) and (100) surface Brillouin zone along with high-symmetry points. The three symmetry-equivalent mirror planes \mathcal{M}_{100} , \mathcal{M}_{010} , and \mathcal{M}_{110} are highlighted with green shading.

guiding principle, we identify here the SrIn_2As_2 class of Zintl materials with the general formula AM_2X_2 (A = alkali, alkaline earth, or rare earth; M = post-transition metal; and X = group IV or V element) in $P6_3/mmc$ space group as a materials family that can support magnetic and nonmagnetic topological phases with substantial flexibility of manipulation through external controls. The Zintl family has attracted great interest since its discovery owing to its fascinating electronic, topological, and magnetic properties [33–43].

In Figs. 1(a)–1(f), we demonstrate the evolution of surface states in three distinct topological phases that could emerge by breaking symmetries with the magnetic orders considering SrIn_2As_2 and EuIn_2As_2 as the representative materials. SrIn_2As_2 is nonmagnetic whereas EuIn_2As_2 is an A -type antiferromagnetic (AFM) system with a Néel temperature of 16 K [36]. SrIn_2As_2 preserves the time-reversal and spatial symmetries of space group $P6_3/mmc$. It is found to be a dual topological insulator with $Z_2 = 1$ and mirror Chern number $C_M = -1$ similar to the Bi_2Te_3 class of topological insulators [44]. The associated Dirac cone states are thus pinned to the Γ point [Figs. 1(a) and 1(d)]. Introducing the AFM order with magnetic moment $m||a$ (aAFM) breaks the time-reversal symmetry but preserves the spatial mirror symmetries (see details below). Thus, the aAFM state realizes a topological

crystalline insulator in which the Dirac cone states are unpinned from the Γ point to lie on the mirror invariant line [Figs. 1(b) and 1(e)]. Considering the out-of-plane AFM with magnetic moment $m||c$ (cAFM), the Dirac cone states are fully gapped, realizing an axion or high-order topological insulator state [Figs. 1(c) and 1(f)]. In this way, a variety of topological states can emerge from the parent materials when the symmetries are relaxed.

II. METHODS

We performed first-principles calculations within the framework of the density functional theory (DFT) using the Vienna *ab initio* simulation package (VASP) [45,46]. The generalized gradient approximation (GGA) [47] with Perdew-Burke-Ernzerhof (PBE) parametrization was used for treating exchange-correlation effects. $\text{Eu } f$ electrons were taken as valence electrons and we used the GGA+ U [48,49] scheme with $U_{\text{eff}} = 5.0$ eV for $\text{Eu } f$ states to include strong electron correlation effects. A kinetic energy cutoff of 350 eV for the plane-wave basis set and a Γ -centered $9 \times 9 \times 9$ k mesh [50] for bulk Brillouin zone (BZ) integrations were used. We consider fully relaxed structural parameters to compute the electronic structure [see Supplemental Material (SM) for details [51]]. The bulk topological properties and surface spectral functions were calculated using the WANNIERTOOLS software package [52].

III. RESULTS AND DISCUSSION

A. Crystal structure and symmetries

The crystal lattice of AM_2X_2 Zintl compounds is described by the hexagonal space group $P6_3/mmc$ (No. 194) with the atomic arrangement illustrated in Figs. 1(g) and 1(h) for SrIn_2As_2 as an example [33,35,37]. The Sr, In, and As atoms occupy Wyckoff $2a$, $4f$, and $4f$ positions, respectively. This crystal contains covalently bonded two-dimensional (2D) networks of SrIn_2As_2 along the hexagonal c axis. Each SrIn_2As_2 2D network contains $[\text{In}_2\text{As}_2]^{2-}$ anion layers which are balanced by Sr^{2+} cation layers. The number of valence electrons thus obeys the octet rule with filled valence shells ($d^{10}s^2p^6$), leading to a semiconducting or semimetallic ground state. The Sr atoms can be replaced with other divalent rare-earth magnetic atoms such as Eu to realize magnetic compounds as reported in experiments [42]. The crystal lattice contains symmetries generated by an inversion center \mathcal{I} , twofold rotation axes \mathcal{C}_{2y} and $\mathcal{G}_{2x} = \{\mathcal{C}_{2x}|00\frac{1}{2}\}$, twofold screw rotation axis $\mathcal{G}_{2z} = \{\mathcal{C}_{2z}|00\frac{1}{2}\}$, and a threefold rotation axis \mathcal{C}_{3z} . These symmetry generators result in 24 symmetry operators including a sixfold screw rotation $\{\mathcal{C}_{6z}|00\frac{1}{2}\}$ ($\mathcal{C}_{3z} \otimes \{\mathcal{C}_{2z}|00\frac{1}{2}\}$), symmetry-equivalent vertical mirror \mathcal{M}_{100} and glide-mirror $\{\mathcal{M}_{120}|00\frac{1}{2}\}$ planes, and a horizontal mirror plane $\{\mathcal{M}_{001}|00\frac{1}{2}\}$. Figure 1(i) shows the bulk BZ and the (001) and (100) surface-projected BZs where various high-symmetry points are marked.

B. Nonmagnetic topological states

Topological states can be identified by an inverted band structure owing to the high spin-orbit coupling (SOC) or

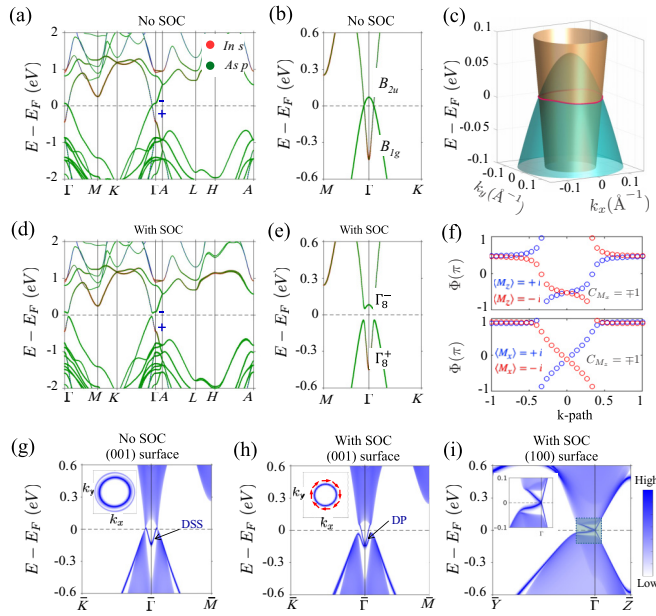


FIG. 2. Topological band structure of nonmagnetic SrIn_2As_2 . (a) Calculated bulk band structure without spin-orbit coupling (SOC). The parity eigenvalues (\pm) and the In s (red) and As p (green) orbitals are marked. (b) Closeup of the bands along the Γ - K and Γ - M directions in the $k_z = 0$ plane. Band crossings between the B_{1g} and B_{2u} states with opposite M_z mirror eigenvalues are evident. (c) E - k_x - k_y rendition of the valence and conduction bands on the $k_z = 0$ plane. The nodal line is marked with the red line. (d), (e) Same as (a), (b) but with the inclusion of SOC. A hybridization gap between the valence and conduction bands is seen. (f) Evolution of the Wannier charge center on the $k_z = 0$ and $k_x = 0$ planes. The nonzero mirror Chern number confirms the mirror TCI phase in SrIn_2As_2 . (g), (h) Band structure of (001) surface without and with SOC. The inset shows the Fermi contours associated with the calculated surface states. (i) Surface band structure of (100) surface with SOC. The symmetry-enforced anisotropic Dirac cone is highlighted in the inset.

crystal field effects. The bulk band structure and band symmetries of SrIn_2As_2 in the absence of SOC are shown in Fig. 2(a). A band inversion is seen between the B_{1g} and B_{2u} states at the Γ point [Fig. 2(b)]. An orbital analysis shows that the B_{1g} states are derived from the In s orbitals and lie below the As p orbital derived B_{2u} states. This band order remains normal at other high-symmetry points in BZ. Away from the Γ point, B_{1g} and B_{2u} states are seen to cross on the Γ - M and Γ - K lines at $k = 0.0035$ and 0.0049 \AA^{-1} , respectively. A full BZ exploration shows that these band crossings trace a topological Dirac nodal line on the $k_z = 0$ plane as shown in Fig. 2(c). SrIn_2As_2 thus realizes a band-inversion, topological-nodal-line semimetal without SOC. We have verified the robustness of this topological state via further computations using the hybrid density functional [51].

The band structure in the presence of SOC [Fig. 2(d)] shows a continuous gap between the Γ_8^+ and Γ_8^- states at the Fermi level. Figure 2(e) shows the closeup of the bands along the Γ - M and Γ - K directions and highlights band anti-crossings, and that the SOC drives the system into an inverted insulator state. Since the system preserves inversion symmetry \mathcal{I} , the parity analysis at the eight time-reversal invariant

momentum (TRIM) points gives $Z_2 = (1; 000)$. On the other hand, the \mathcal{M}_{001} and \mathcal{M}_{110} mirror Chern numbers on the $k_z = 0$ and $k_y = 0$ planes are -1 and -1 , respectively, from the Wannier charge center evolution as shown in Fig. 2(f). SrIn_2As_2 is thus a dual topological insulator.

The nontrivial bulk topological properties are of course reflected in the surface band structure. From the (001) surface energy dispersion in Fig. 2(h), a topological Dirac cone state with the Dirac point at the $\bar{\Gamma}$ point can be seen. The associated constant energy contours are circular with an isotropic energy dispersion near the Dirac node and develop a hexagonal shape as one moves away from the Dirac point. The spin texture is helical with a left-handed chirality for the upper Dirac cone [see the inset of Fig. 2(h)]. This surface state is protected by both the time-reversal and \mathcal{M}_{001} mirror symmetry. We also get a similar protected topological state on the low-symmetry (100) side surface. However, the Dirac cone on the (100) surface is located well within the bulk energy gap [Fig. 2(i)]. It has an anisotropic energy dispersion, indicating that the surface Dirac fermions possess an anisotropic velocity distribution.

C. Magnetic topological states

We now consider the topological state of EuIn_2As_2 , which is a magnetic counterpart of SrIn_2As_2 . Notably, $\text{EuIn}_2(\text{As}, \text{P})_2$ is isostructural and isovalent to SrIn_2As_2 but realizes an AFM state below 16 K [36]. EuIn_2As_2 shows immense potential for realizing the axion insulator state and for this reason it has attracted recent attention [38–41]. Neutron diffraction experiments reveal a low-symmetry helical antiferromagnetic order in EuIn_2As_2 , which makes it amenable for realizing various topological states under an external magnetic field [41]. The experimental saturated magnetic moment for Eu ions is $\sim 7.0 \mu_B$ that is close to the magnetic moment of the f^7 state and our calculated value of $6.90 \mu_B$. This indicates that the Eu oxidation state is $+2$, which is similar to the oxidation state of Sr. A tunable $\text{Sr}_{1-x}\text{Eu}_x\text{In}_2(\text{As}, \text{P})_2$ system can thus realize distinct topological magnetic states [42,43]. The dependence of the band gap on the lattice constant [Fig. 3(a)] shows that EuIn_2As_2 has an intrinsically inverted band structure whereas EuIn_2P_2 has a trivial band structure.

Figure 3 shows the topological states of antiferromagnetic $\text{EuIn}_2(\text{As}, \text{P})_2$. We consider topological states originating from the formation of commensurate AFM order in EuIn_2As_2 with the intralayer ferromagnetic coupling and interlayer antiferromagnetic coupling between the Eu spins. The calculated energy for the aAFM is nearly the same as cAFM, making both these states energetically favorable. These nearly degenerate magnetic orders suggest that an external magnetic tuning of the topological state in EuIn_2As_2 would be possible [39–41].

We emphasize that the AFM order reduces the nonmagnetic D_{6h} point-group symmetry to either D_{2h} or D_{3d} depending on the magnetic configuration of the AFM state. Figure 3(b) shows the band structure of AFM EuIn_2As_2 without SOC. It retains the characteristic inverted band features seen in SrIn_2As_2 along with the Dirac nodal line in the BZ. Specifically, the states close to the Fermi level are comprised of In s and As p orbitals, whereas Eu f states provide the

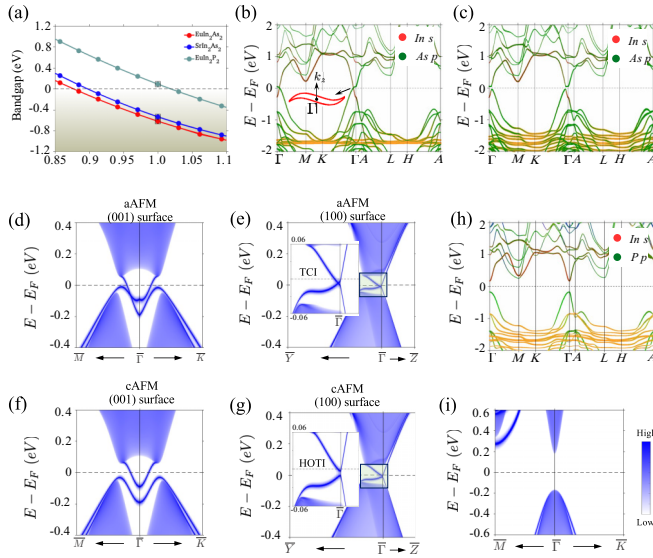


FIG. 3. Topological states and magnetic tunability of antiferromagnetic $\text{EuIn}_2(\text{As}, \text{P})_2$. (a) Variation of the band gap as a function of the relative volume at the Γ point in AFM $\text{EuIn}_2(\text{As}, \text{P})_2$ and nonmagnetic SrIn_2As_2 . Open markers at $V/V_0 = 1$ show the band gap of their pristine states. A topological phase transition from the nontrivial to trivial phase can be achieved by decreasing the volume. Calculated band structure of AFM EuIn_2As_2 (b) without and (c) with SOC. The crossings in (b) form a nodal line unhooked from the $k_z = 0$ plane due to the breaking of \mathcal{M}_{001} the mirror plane symmetry. A hybridization gap opens up at the crossing points and an axion insulator state with $Z_4 = 2$ develops with SOC. The calculated surface band structure of aAFM EuIn_2As_2 for (d) (001) and (e) (100) surfaces. The mirror symmetry-protected Dirac cone states are seen inside the bulk gap. (f), (g) Same as (d), (e) but for cAFM order. The topological surface states are now gapped with a magnetic gap at the $\bar{\Gamma}$ point. (h), (i) Calculated (h) bulk and (i) (001) surface band structure of aAFM EuIn_2P_2 . A trivial insulating state with $Z_4 = 0$ is resolved.

necessary exchange coupling for inducing the magnetism. Often strong electron correlations in Eu f states affect band orderings and thus the topological state of the material [53–55]. Our analysis by varying Hubbard U_{eff} in GGA+ U in parallel with hybrid functional calculations reveals that states close to the Fermi level and the topological phase of EuIn_2As_2 are not sensitive to the choice of U [51]. However, magnetism breaks the horizontal \mathcal{M}_{001} mirror plane, and thus unlike nonmagnetic SrIn_2As_2 , the nodal line in EuIn_2As_2 for a particular spin is unhooked from the $k_z = 0$ plane and wiggles in the momentum space around the Γ point with small k_z dispersion [Fig. 3(b)]. The inclusion of SOC in computations develops a gap at the band-crossing points, separating valence and conduction bands in both the aAFM and cAFM states [Fig. 3(c)]. Since both these AFM states preserve inversion \mathcal{I} symmetry, we access their topological character by calculating the parity-based Z_4 topological invariant. The calculated Z_4 is 2, indicating that EuIn_2As_2 realizes an axion insulator state. Notably, despite a nonzero Z_4 invariant, the topological state of the system can be further classified based on the magnetic group symmetries as discussed below.

The aAFM state of EuIn_2As_2 preserves \mathcal{M}_{001} and \mathcal{M}_{100} mirror planes. The calculated mirror Chern number on the $k_z = 0$ and $k_y = 0$ planes is -1 , similar to SrIn_2As_2 . EuIn_2As_2 is thus a mirror topological crystalline insulator with aAFM order. This is further manifested in the surface spectrum on the (001) and (100) planes where Dirac cones are seen along the mirror invariant lines. Specifically, the mirror-protected Dirac cone is located on the $\bar{\Gamma}-\bar{M}$ line in the (001) plane and $\bar{\Gamma}-\bar{Y}$ line in the (100) plane as depicted in Figs. 3(d) and 3(e). In the cAFM state, both the \mathcal{M}_{001} and \mathcal{M}_{100} mirror planes are broken and no symmetry-protected Dirac cone is found on either surface. Instead, a magnetic gap develops at the surface-Dirac-node crossings [Figs. 3(f) and 3(g)]. The system thus realizes a higher-order topological insulator with conducting hinge states. Figures 3(h) and 3(i) show the bulk and surface band structures of AFM EuIn_2P_2 . In contrast to EuIn_2As_2 , EuIn_2P_2 exhibits a trivial state with $Z_4 = 0$. This trivial state may arise due to strong carrier confinement. EuIn_2P_2 has a relatively smaller unit cell volume (267.03 \AA^3) compared to EuIn_2As_2 (290.77 \AA^3), which could induce a strong carrier confinement effect. Such effects reduce the bandwidth for both the valence and conduction bands, and result in the avoidance of a band inversion in the vicinity of the Fermi level.

To showcase the physics that emerges in the presence of an external magnetic field, we now discuss the topological states in ferromagnetic (FM) $\text{EuIn}_2(\text{As}, \text{P})_2$. Our total energy calculations show that the FM state is ~ 2 (3) meV/unit cell higher than the AFM state of EuIn_2As_2 (EuIn_2P_2). Notably, we have considered the commensurate FM orders with the magnetic moment $m||a$ (aFM) and magnetic moment $m||c$ (cFM). aFM and cFM states are nearly degenerate with an energy similar to that of the AFM state. It is thus possible that FM order in these materials becomes energetically favorable under a small external magnetic field. For FM EuIn_2As_2 , we find that the bulk band inversion stays robust for both the FM orders and the system realizes an axion insulator state with $Z_4 = 2$ [51].

Figure 4 illustrates the bulk and surface band structure of FM EuIn_2P_2 . Due to the large exchange coupling of Eu f states, it shows a single spin-band inversion in both aFM and cFM orders. The parity-based topological indicator is found to be $Z_4 = 1$, indicating that the system is a nontrivial half semimetal. Since this type of topological semimetal state of a magnetic system depends on crystalline symmetries, one can realize both the time-reversal-broken Weyl semimetal or the nodal-line semimetal state. The aFM state breaks \mathcal{M}_{100} mirror plane symmetry, and the system realizes an ideal Weyl semimetal with two Weyl nodes in the bulk BZ, as shown in Fig. 4(a). The Weyl nodes are located on the $k_z = 0$ plane at $(0.000, 0.0355, 0.0) \text{ \AA}^{-1}$ with chirality $+1$ and at $(0.000, -0.0355, 0.0) \text{ \AA}^{-1}$ with chirality -1 (see SM for details [51]). The surface band structure and the surface Fermi arcs connecting the projected Weyl nodes on the (001) surface are shown in Figs. 4(b) and 4(c). Figures 4(d)–4(f) show the bulk and surface electronic spectrum of the cFM state. Since the cFM state preserves the \mathcal{M}_{001} mirror symmetry, the two crossing bands in Fig. 4(d) stay robust against band hybridization, thereby realizing a single Weyl nodal line on the $k_z = 0$ plane. The associated nontrivial drumhead surface states and Fermi contours are shown in Figs. 4(e) and 4(f).

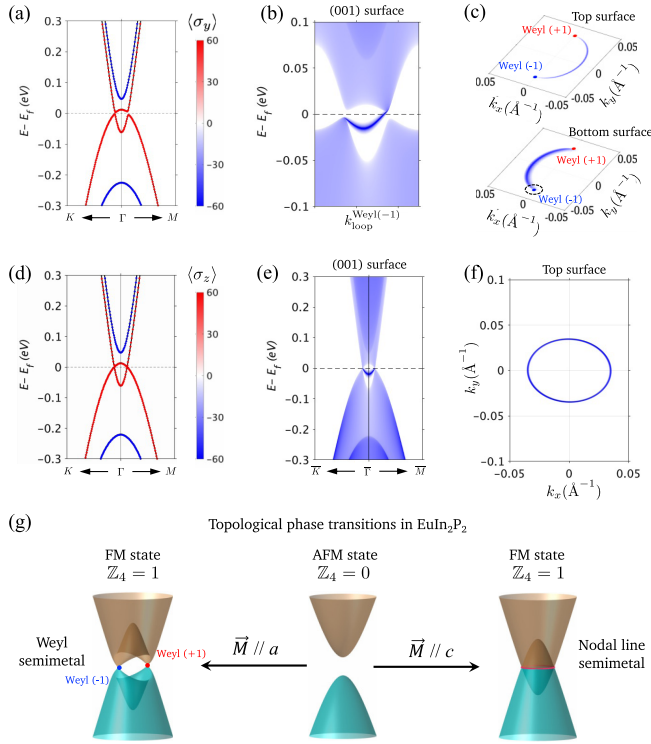


FIG. 4. Ferromagnetic tunability of topological states of EuIn_2P_2 . (a) Calculated spin-resolved bulk band structure of A-type ferromagnetic (aFM) configuration. A single spin-band inversion drives the aFM phase into an ideal ferromagnetic Weyl semimetal with a pair of Weyl nodes on the k_x - k_y plane. (b) The surface band structure calculated along the circular path shown in (c) on the (001) surface enclosing a Weyl point. The chiral surface states are seen connecting the projected bulk valence and conduction bands. (c) The Fermi-arc surface states, connecting projected Weyl nodes on the top and bottom surfaces. (d) Spin-resolved bulk and (e) (001) surface band structure of C-type ferromagnetic (cFM) configuration. The presence of \mathcal{M}_{001} mirror plane in the cFM configuration protects the crossing bands to hybridize, realizing a nodal line with a drumhead surface state. (f) The associated Fermi band contours showing the drumhead surface states. (g) Schematic representation of the trival insulator ($Z_4 = 0$) to a Weyl semimetal or nodal-line semimetal ($Z_4 = 1$) transition in EuIn_2P_2 with applied external magnetic field.

We emphasize that an FM state can be considered as a fully polarized final state of an initial AFM state. It is thus possible to realize the aforementioned ideal topological half-semimetal states in EuIn_2P_2 . This is shown schematically in Fig. 4(g). A magnetic field applied parallel to the y axis will drive it into a nearly ideal Weyl semimetal whereas a magnetic field applied parallel to the z axis will drive it into a Weyl nodal-line semimetal.

IV. $k \cdot p$ MODEL ANALYSIS

The preceding analysis reveals that the band inversion happens between In s and As p states at Γ in both the nonmagnetic and magnetic compounds. The role of magnetism is to reduce the symmetries and drive the system into various TCI states. We can thus consider the Hamiltonian of the nonmag-

netic state and regard magnetism as perturbation allowed by the magnetic symmetries so that $H = H_0 + \Delta H$, where H_0 is the nonmagnetic state Hamiltonian and ΔH originates from the magnetic order. The irreducible representations of two bands at Γ close to the Fermi level are B_{1g} and B_{2u} of the symmetry group D_{6h} as shown in Fig. 1(b). Based on the theory of invariants, the low-energy effective Hamiltonian can then be described as

$$H_0(\vec{k}) = \epsilon(\vec{k})\tau_0\sigma_0 + A_1\tau_x(k_x\sigma_y - k_y\sigma_x) + A_2k_z\tau_y\sigma_0 + M(\vec{k})\tau_z\sigma_0, \quad (1)$$

where $\epsilon(\vec{k}) = \epsilon_0 + \epsilon_1(k_x^2 + k_y^2) + \epsilon_2k_z^2$ and $M(\vec{k}) = M_0 - \beta_1(k_x^2 + k_y^2) - \beta_2k_z^2$. τ and σ are the Pauli spin matrices in the orbital and spin space, respectively, and M_0 , β_1 , and $\beta_2 > 0$ [51]. When SOC is off, $A_1 = 0$, which leads to a nodal ring in the $k_z = 0$ plane described by $k_x^2 + k_y^2 = M_0/\beta_1$. A cAFM order that breaks \mathcal{T} , \mathcal{C}_{2y} , and \mathcal{G}_{2z} while preserving $\mathcal{TC}_{2y} = \tau_z\sigma_0\mathcal{K}$ and $\mathcal{C}_{2y}\mathcal{G}_{2z} = \mathcal{G}_{2x}$ symmetry operations yields

$$\Delta H_{\text{cAFM}}(\vec{k}) = (B_1\tau_0 + B_2\tau_z)[(k_x^2 - k_y^2)\sigma_x - 2k_xk_y\sigma_y]. \quad (2)$$

An aAFM order that breaks \mathcal{T} and \mathcal{C}_{3z} gives

$$\Delta H_{\text{aAFM}}(\vec{k}) = D_0\tau_y(k_x\sigma_y - \delta_\epsilon k_y\sigma_x). \quad (3)$$

The ferromagnetic cFM and aFM phases can come with $\Delta H_{\text{cFM}} = \lambda_c\tau_z\sigma_z$ and $\Delta H_{\text{aFM}} = \lambda_a\tau_z\sigma_y$, respectively.

V. SUMMARY

We have shown that the interplay of topology, symmetry, and magnetism in the experimentally realized SrIn_2As_2 materials class can enable access to a multitude of topological states through the lowering of symmetry via various magnetic configurations. SrIn_2As_2 , a hexagonal Zintl compound, is found to be a dual topological insulator with nontrivial $Z_2 = 1$ and mirror Chern number $C_M = -1$. Its isostructural and isovalent magnetic cousin $\text{EuIn}_2(\text{As}, \text{P})_2$ supports a variety of topological states. Remarkably, we find that EuIn_2As_2 is an axion insulator with $Z_4 = 2$, which can also realize a mirror topological magnetic insulator for aAFM (magnetic moment $m||a$) and a higher-order topological insulator for cAFM ($m||c$). In contrast, EuIn_2P_2 is a robust AFM trivial insulator in its pristine form and undergoes a magnetic-field-driven transition to an ideal ferromagnetic Weyl point ($m||a$) and a Weyl nodal-line ($m||c$) half semimetal with $Z_4 = 1$. In conjunction with the bulk topological states, we also obtain a variety of surface states, viz., gapless or gapful, pinned or unpinned at the Γ point [see Table I for a summary of topological states in $(\text{Sr}, \text{Eu})\text{In}_2(\text{As}, \text{P})_2$]. Since Sr and Eu are isovalent, $\text{Sr}_{1-x}\text{Eu}_x\text{In}_2(\text{As}, \text{P})_2$ provides a material that can be tuned systematically between various topological orders through its inherent magnetism and external stimuli. A topological phase transition from an axion insulator ($Z_4 = 2$) to a trivial insulator ($Z_4 = 0$) can be realized in $\text{EuIn}_2\text{As}_{2-x}\text{P}_x$ by varying the doping x [51]. Our results thus highlight that the SrIn_2As_2 class of topological insulators in the Zintl family are a promising materials platform for investigating the interplay of topology, symmetry, and magnetism and for device applications.

TABLE I. Summary of topological states in SrIn_2As_2 , EuIn_2As_2 , and EuIn_2P_2 Zintl materials for different commensurate magnetic configurations. NM stands for nonmagnetic, aAFM (cAFM) denotes an antiferromagnetic state with magnetic moment $m||a$ ($m||c$), and aFM (cFM) represents a ferromagnetic state with magnetic moment $m||a$ ($m||c$). TI, TCI, AI, and NI stand for topological insulator, topological crystalline insulator, axion insulator, and normal insulator, respectively. WSM and NLSM denote Weyl semimetal and nodal-line semimetal, respectively. See text for details.

Compound	Magnetic state	Space group	Topological invariant	Topological state
SrIn_2As_2	NM	$P6_3/mmc$	$Z_2 = 1$	TI and TCI
EuIn_2As_2	aAFM	$Cmcm$	$Z_4 = 2$	TCI
	cAFM	$P6_3/m'm'c$	$Z_4 = 2$	AI
	aFM	$Cmc'm'$	$Z_4 = 2$	TCI
	cFM	$P6_3/mm'c'$	$Z_4 = 2$	AI
EuIn_2P_2	aAFM	$Cmcm$	$Z_4 = 0$	NI
	cAFM	$P6_3/m'm'c$	$Z_4 = 0$	NI
	aFM	$Cmc'm'$	$Z_4 = 1$	WSM
	cFM	$P6_3/mm'c'$	$Z_4 = 1$	NLSM

ACKNOWLEDGMENTS

A.B.S. acknowledges IIT Kanpur for providing support from a Senior Research Fellowship. A.B.S. and A.A. thank the CC-IITK for providing the HPC facility. A.A. acknowledge funding from Science Education and Research Board (SERB) and Department of Science and Technology (DST), Government of India. T.-R.C. was supported by the Young Scholar Fellowship Program from the Ministry of Science and Technology (MOST) in Taiwan, under a MOST grant for the Columbus Program MOST110-2636-M-006-016, NCKU, Taiwan, and National Center for Theoretical Sciences, Taiwan. Work at NCKU was supported by the MOST, Taiwan, under Grant No. MOST107-2627-E-006-001 and Higher

Education Sprout Project, Ministry of Education to the Headquarters of University Advancement at NCKU. S.M.H. is supported by the MOST-AFOSR program on Topological and Nanostructured Materials, Grant No. 110-2124-M-110-002-MY3. H.L. acknowledges the support by the Ministry of Science and Technology (MOST) in Taiwan under Grant No. MOST 109-2112-M-001-014-MY3. The work at Northeastern University was supported by the Air Force Office of Scientific Research under Award No. FA9550-20-1-0322 and benefited from the computational resources of Northeastern University's Advanced Scientific Computation Center (ASCC) and the Discovery Cluster. The work at TIFR Mumbai was supported by the Department of Atomic Energy of the Government of India under Project No. 12-R&D-TFR-5.10-0100.

- [1] M. Z. Hasan and C. L. Kane, Colloquium: Topological insulators, *Rev. Mod. Phys.* **82**, 3045 (2010).
- [2] X.-L. Qi and S.-C. Zhang, Topological insulators and superconductors, *Rev. Mod. Phys.* **83**, 1057 (2011).
- [3] A. Bansil, H. Lin, and T. Das, Colloquium: Topological band theory, *Rev. Mod. Phys.* **88**, 021004 (2016).
- [4] N. P. Armitage, E. J. Mele, and A. Vishwanath, Weyl and Dirac semimetals in three-dimensional solids, *Rev. Mod. Phys.* **90**, 015001 (2018).
- [5] L. Fu, Topological Crystalline Insulators, *Phys. Rev. Lett.* **106**, 106802 (2011).
- [6] T. H. Hsieh, H. Lin, J. Liu, W. Duan, A. Bansil, and L. Fu, Topological crystalline insulators in the SnTe material class, *Nat. Commun.* **3**, 982 (2012).
- [7] C. Fang and L. Fu, New classes of topological crystalline insulators having surface rotation anomaly, *Sci. Adv.* **5**, eaat2374 (2019).
- [8] B. Wang, B. Singh, B. Ghosh, W.-C. Chiu, M. M. Hosen, Q. Zhang, L. Ying, M. Neupane, A. Agarwal, H. Lin, and A. Bansil, Topological crystalline insulator state with type-II Dirac fermions in transition metal dipnictides, *Phys. Rev. B* **100**, 205118 (2019).
- [9] F. Schindler, A. M. Cook, M. G. Vergniory, Z. Wang, S. S. P. Parkin, B. A. Bernevig, and T. Neupert, Higher-order topological insulators, *Sci. Adv.* **4**, eaat0346 (2018).
- [10] F. Schindler, Z. Wang, M. G. Vergniory, A. M. Cook, A. Murani, S. Sengupta, A. Y. Kasumov, R. Deblock, S. Jeon, I. Drozdov, H. Bouchiat, S. Guéron, A. Yazdani, B. A. Bernevig, and T. Neupert, Higher-order topology in bismuth, *Nat. Phys.* **14**, 918 (2018).
- [11] Z. K. Liu, J. Jiang, B. Zhou, Z. J. Wang, Y. Zhang, H. M. Weng, D. Prabhakaran, S.-K. Mo, H. Peng, P. Dudin, T. Kim, M. Hoesch, Z. Fang, X. Dai, Z. X. Shen, D. L. Feng, Z. Hussain, and Y. L. Chen, A stable three-dimensional topological Dirac semimetal Cd_3As_2 , *Nat. Mater.* **13**, 677 (2014).
- [12] Z. K. Liu, B. Zhou, Y. Zhang, Z. J. Wang, H. M. Weng, D. Prabhakaran, S.-K. Mo, Z. X. Shen, Z. Fang, X. Dai, Z. Hussain, and Y. L. Chen, Discovery of a three-dimensional topological Dirac semimetal, Na_3Bi , *Science* **343**, 864 (2014).
- [13] B. Singh, S. Mardanya, C. Su, H. Lin, A. Agarwal, and A. Bansil, Spin-orbit coupling driven crossover from a starfruitlike nodal semimetal to Dirac and Weyl semimetal state in CaAuAs , *Phys. Rev. B* **98**, 085122 (2018).
- [14] S.-Y. Xu, I. Belopolski, N. Alidoust, M. Neupane, G. Bian, C. Zhang, R. Sankar, G. Chang, Z. Yuan, C.-C. Lee, S.-M. Huang,

- H. Zheng, J. Ma, D. S. Sanchez, B. Wang, A. Bansil, F. Chou, P. P. Shibayev, H. Lin, S. Jia *et al.*, Discovery of a Weyl fermion semimetal and topological Fermi arcs, *Science* **349**, 613 (2015).
- [15] B. Q. Lv, H. M. Weng, B. B. Fu, X. P. Wang, H. Miao, J. Ma, P. Richard, X. C. Huang, L. X. Zhao, G. F. Chen, Z. Fang, X. Dai, T. Qian, and H. Ding, Experimental discovery of Weyl semimetal TaAs, *Phys. Rev. X* **5**, 031013 (2015).
- [16] S.-Y. Xu, N. Alidoust, G. Chang, H. Lu, B. Singh, I. Belopolski, D. S. Sanchez, X. Zhang, G. Bian, H. Zheng, M.-A. Husanu, Y. Bian, S.-M. Huang, C.-H. Hsu, T.-R. Chang, H.-T. Jeng, A. Bansil, T. Neupert, V. N. Strocov, H. Lin *et al.*, Discovery of Lorentz-violating type II Weyl fermions in LaAlGe, *Sci. Adv.* **3**, e1603266 (2017).
- [17] Z. Wang, A. Alexandradinata, R. J. Cava, and B. A. Bernevig, Hourglass fermions, *Nature (London)* **532**, 189 (2016).
- [18] B. Singh, B. Ghosh, C. Su, H. Lin, A. Agarwal, and A. Bansil, Topological Hourglass Dirac Semimetal in the Nonpolar Phase of Ag_2BiO_3 , *Phys. Rev. Lett.* **121**, 226401 (2018).
- [19] B. Bradlyn, J. Cano, Z. Wang, M. G. Vergniory, C. Felser, R. J. Cava, and B. A. Bernevig, Beyond Dirac and Weyl fermions: Unconventional quasiparticles in conventional crystals, *Science* **353**, aaf5037 (2016).
- [20] S. Mardanya, B. Singh, S.-M. Huang, T.-R. Chang, C. Su, H. Lin, A. Agarwal, and A. Bansil, Prediction of threefold fermions in a nearly ideal Dirac semimetal BaAgAs, *Phys. Rev. Materials* **3**, 071201(R) (2019).
- [21] Z. Song, T. Zhang, Z. Fang, and C. Fang, Quantitative mappings between symmetry and topology in solids, *Nat. Commun.* **9**, 3530 (2018).
- [22] B. Bradlyn, L. Elcoro, J. Cano, M. G. Vergniory, Z. Wang, C. Felser, M. I. Aroyo, and B. A. Bernevig, Topological quantum chemistry, *Nature (London)* **547**, 298 (2017).
- [23] T. Jungwirth, X. Marti, P. Wadley, and J. Wunderlich, Antiferromagnetic spintronics, *Nat. Nanotechnol.* **11**, 231 (2016).
- [24] J. E. Moore, Optical properties of Weyl semimetals, *Natl. Sci. Rev.* **6**, 206 (2019).
- [25] R. S. K. Mong, A. M. Essin, and J. E. Moore, Antiferromagnetic topological insulators, *Phys. Rev. B* **81**, 245209 (2010).
- [26] M. M. Otrokov, I. I. Klimovskikh, H. Bentmann, D. Estyunin, A. Zeugner, Z. S. Aliev, S. Gaß, A. U. B. Wolter, A. V. Koroleva, A. M. Shikin, M. Blanco-Rey, M. Hoffmann, I. P. Rusinov, A. Y. Vyazovskaya, S. V. Ereemeev, Y. M. Koroteev, V. M. Kuznetsov, F. Freyse, J. Sánchez-Barriga, I. R. Amiraslanov *et al.*, Prediction and observation of an antiferromagnetic topological insulator, *Nature (London)* **576**, 416 (2019).
- [27] J. Li, Y. Li, S. Du, Z. Wang, B.-L. Gu, S.-C. Zhang, K. He, W. Duan, and Y. Xu, Intrinsic magnetic topological insulators in van der Waals layered MnBi_2Te_4 -family materials, *Sci. Adv.* **5**, eaaw5685 (2019).
- [28] C. Hu, L. Ding, K. N. Gordon, B. Ghosh, H.-J. Tien, H. Li, A. G. Linn, S.-W. Lien, C.-Y. Huang, S. Mackey, J. Liu, P. V. S. Reddy, B. Singh, A. Agarwal, A. Bansil, M. Song, D. Li, S.-Y. Xu, H. Lin, H. Cao *et al.*, Realization of an intrinsic ferromagnetic topological state in $\text{MnBi}_8\text{Te}_{13}$, *Sci. Adv.* **6**, eaba4275 (2020).
- [29] I. Belopolski, K. Manna, D. S. Sanchez, G. Chang, B. Ernst, J. Yin, S. S. Zhang, T. Cochran, N. Shumiya, H. Zheng, B. Singh, G. Bian, D. Multer, M. Litskevich, X. Zhou, S.-M. Huang, B. Wang, T.-R. Chang, S.-Y. Xu, A. Bansil *et al.*, Discovery of topological Weyl fermion lines and drumhead surface states in a room temperature magnet, *Science* **365**, 1278 (2019).
- [30] J.-X. Yin, N. Shumiya, Y. Jiang, H. Zhou, G. Macam, H. O. M. Sura, S. S. Zhang, Z.-J. Cheng, Z. Guguchia, Y. Li, Q. Wang, M. Litskevich, I. Belopolski, X. P. Yang, T. A. Cochran, G. Chang, Q. Zhang, Z.-Q. Huang, F.-C. Chuang, H. Lin *et al.*, Spin-orbit quantum impurity in a topological magnet, *Nat. Commun.* **11**, 4415 (2020).
- [31] L.-L. Wang, H. C. Po, R.-J. Slager, and A. Vishwanath, Topological descendants of a multicritical Dirac semimetal with magnetism and strain, *Phys. Rev. B* **104**, 165107 (2021).
- [32] B. Singh, H. Lin, R. Prasad, and A. Bansil, Topological phase transition and two-dimensional topological insulators in Ge-based thin films, *Phys. Rev. B* **88**, 195147 (2013).
- [33] J. Jiang and S. M. Kauzlarich, Colossal magnetoresistance in a rare earth Zintl compound with a new structure type: EuIn_2P_2 , *Chem. Mater.* **18**, 435 (2006).
- [34] J. Mathieu, R. Achey, J.-H. Park, K. M. Purcell, S. W. Tozer, and S. E. Lattner, Flux growth and electronic properties of $\text{Ba}_2\text{In}_5\text{Pn}_5$ ($\text{Pn} = \text{P}, \text{As}$): Zintl phases exhibiting metallic behavior, *Chem. Mater.* **20**, 5675 (2008).
- [35] J. F. Rauscher, C. L. Condon, T. Beault, S. M. Kauzlarich, N. Jensen, P. Klavins, S. MaQuilon, Z. Fisk, and M. M. Olmstead, Flux growth and structure of two compounds with the EuIn_2P_2 structure type, AlIn_2P_2 ($A = \text{Ca}$ and Sr), and a new structure type, BaIn_2P_2 , *Acta Crystallogr., Sect. C* **65**, i69 (2009).
- [36] A. M. Goforth, P. Klavins, J. C. Fettinger, and S. M. Kauzlarich, Magnetic properties and negative colossal magnetoresistance of the rare earth Zintl phase EuIn_2As_2 , *Inorg. Chem.* **47**, 11048 (2008).
- [37] N. Guechi, A. Bouhemadou, A. Guechi, M. Reffas, L. Louail, A. Bourzami, M. Chegaar, and S. Bin-Omran, First-principles prediction of the structural, elastic, electronic and optical properties of the Zintl phases MIn_2P_2 ($M = \text{Ca}, \text{Sr}$), *J. Alloys Compd.* **577**, 587 (2013).
- [38] Y. Xu, Z. Song, Z. Wang, H. Weng, and X. Dai, Higher-Order Topology of the Axion Insulator EuIn_2As_2 , *Phys. Rev. Lett.* **122**, 256402 (2019).
- [39] Y. Zhang, K. Deng, X. Zhang, M. Wang, Y. Wang, C. Liu, J.-W. Mei, S. Kumar, E. F. Schwier, K. Shimada, C. Chen, and B. Shen, In-plane antiferromagnetic moments and magnetic polaron in the axion topological insulator candidate EuIn_2As_2 , *Phys. Rev. B* **101**, 205126 (2020).
- [40] S. Regmi, M. M. Hosen, B. Ghosh, B. Singh, G. Dhakal, C. Sims, B. Wang, F. Kabir, K. Dimitri, Y. Liu, A. Agarwal, H. Lin, D. Kaczorowski, A. Bansil, and M. Neupane, Temperature-dependent electronic structure in a higher-order topological insulator candidate EuIn_2As_2 , *Phys. Rev. B* **102**, 165153 (2020).
- [41] S. X. M. Riberolles, T. V. Trevisan, B. Kuthanazhi, T. W. Heitmann, F. Ye, D. C. Johnston, S. L. Bud'ko, D. H. Ryan, P. C. Canfield, A. Kreyssig, A. Vishwanath, R. J. McQueeney, L. L. Wang, P. P. Orth, and B. G. Ueland, Magnetic crystalline-symmetry-protected axion electrodynamics and field-tunable unpinned Dirac cones in EuIn_2As_2 , *Nat. Commun.* **12**, 999 (2021).
- [42] Q. Zhang, Y. Xiao, Z. Xu, G. Liu, J. Li, and G. Rao, Eu doping effects on structural and magnetic properties of $(\text{Sr}_{2-x}\text{Eu}_x)\text{FeMoO}_6$ compounds, *J. Solid State Chem.* **183**, 2432 (2010).

- [43] K. Shinozaki, Y. Goto, K. Hoshi, R. Kiyama, N. Nakamura, A. Miura, C. Moriyoshi, Y. Kuroiwa, H. Usui, and Y. Mizuguchi, Thermoelectric properties of the As/P-based Zintl compounds $\text{EuIn}_2\text{As}_{2-x}\text{P}_x$ ($x = 0-2$) and SrSn_2As_2 , *ACS Appl. Energy Mater.* **4**, 5155 (2021).
- [44] T. Rauch, M. Flieger, J. Henk, I. Mertig, and A. Ernst, Dual Topological Character of Chalcogenides: Theory for Bi_2Te_3 , *Phys. Rev. Lett.* **112**, 016802 (2014).
- [45] G. Kresse and J. Furthmüller, Efficient iterative schemes for *ab initio* total-energy calculations using a plane-wave basis set, *Phys. Rev. B* **54**, 11169 (1996).
- [46] G. Kresse and D. Joubert, From ultrasoft pseudopotentials to the projector augmented-wave method, *Phys. Rev. B* **59**, 1758 (1999).
- [47] J. P. Perdew, K. Burke, and M. Ernzerhof, Generalized Gradient Approximation Made Simple, *Phys. Rev. Lett.* **77**, 3865 (1996).
- [48] V. I. Anisimov, J. Zaanen, and O. K. Andersen, Band theory and Mott insulators: Hubbard U instead of Stoner I , *Phys. Rev. B* **44**, 943 (1991).
- [49] V. I. Anisimov, F. Aryasetiawan, and A. I. Lichtenstein, First-principles calculations of the electronic structure and spectra of strongly correlated systems: the LDA + U method, *J. Phys.: Condens. Matter* **9**, 767 (1997).
- [50] H. J. Monkhorst and J. D. Pack, Special points for Brillouin-zone integrations, *Phys. Rev. B* **13**, 5188 (1976).
- [51] See Supplemental Material at <http://link.aps.org/supplemental/10.1103/PhysRevMaterials.6.044204> for bandgap correction, robustness of topology in EuIn_2As_2 with Eu f states correlations, topological states in ferromagnetic $\text{EuIn}_2(\text{As}, \text{P})_2$, topological phase transition in $\text{EuIn}_2\text{As}_{2-x}\text{P}_x$, and detailed $k \cdot p$ model Hamiltonian.
- [52] Q. Wu, S. Zhang, H.-F. Song, M. Troyer, and A. A. Soluyanov, Wanniertools: An open-source software package for novel topological materials, *Comput. Phys. Commun.* **224**, 405 (2018).
- [53] L. I. Bendavid and E. A. Carter, Status in calculating electronic excited states in transition metal oxides from first principles, in *First Principles Approaches to Spectroscopic Properties of Complex Materials*, edited by C. Di Valentin, S. Botti, and M. Cococcioni (Springer, Berlin, 2014), pp. 47–98.
- [54] A. Prokofiev, A. Shelykh, and B. Melekh, Periodicity in the band gap variation of Ln_2X_3 ($X = \text{O}, \text{S}, \text{Se}$) in the lanthanide series, *J. Alloys Compd.* **242**, 41 (1996).
- [55] M. Yu, S. Yang, C. Wu, and N. Marom, Machine learning the Hubbard U parameter in DFT+ U using Bayesian optimization, *npj Comput. Mater.* **6**, 180 (2020).